scatter event rate which averages 820 ± 8 counts per bin, the chance coincidence rate which averages 374 ± 6 counts per bin, and the background scatter event rate of 49 ± 2 counts per bin. These rates were determined and confirmed using event rates before and after the burst, combined with studies of the readout times of multiple detectors during scattered events, and were verified independently using our Monte Carlo simulations. Although the rotation will average out systematic variations in the scatter angle distribution, we still have to correct for the complex time profile of the burst itself, which will cause variations for an unpolarized source owing to the finite number of potential scatter angles RHESSI can measure at any given instant. We modelled this effect by using the 0.15–2.0 MeV total count rate in the RHESSI instrument (Fig. 1) as the time-dependent flux template for a photon transport Monte Carlo simulation, and using the time-averaged GRB photon spectrum as measured by RHESSI for our input spectrum. This simulation used the detailed RHESSI mass model that has been developed under CERN's GEANT package, allowing us to model the instrument response to a GRB at the IPN[8] sky coordinates for each rotation angle and instantaneous flux, assuming an unpolarized source. This distribution is also presented in the top panel of Fig. 2. We are looking for a modulation signal relative to this variation induced by the GRB time profile.

In the bottom panel of Fig. 2 we show the residual of the measured distribution once we have subtracted away the simulated response for an unpolarized GRB, showing our absolute modulation signal. For an unpolarized source we would expect this distribution to be flat, which we can rule out at an extremely high confidence level ($\chi^2 = 83.5$, 11 degrees of freedom, d.f.). When we fit this with a modulation curve, the fit improves significantly ($\chi^2 = 16.9$, 9 d.f.), with an amplitude of 128 ± 16 counts per bin. Statistically, this is a reasonable fit to the data (the probability of $\chi^2 > 16.9$ is 5%), but could be improved with even more detailed Monte Carlo simulations including time-dependent spectral variability. Using the count rates given above and the simulated distribution for an unpolarized GRB, we performed further numerical simulations to determine the probability that an unpolarized GRB could produce a modulation as large as the one we measure due to random Poisson counting statistics. We found this probability to be very low, $<10^{-8}$, which translates to a confidence that we have measured a polarization at a level $>5.7\sigma$. Finally, we estimated the modulation factor to be $\mu_m = 0.19 \pm 0.04$, using both a separate photon transport code which fully treats polarization in scattering and uses a simplified mass model, as well as analytical estimates based on the GEANT simulation with the full RHESSI mass model. Combining the modulation amplitude, the total source scatter event rate, and the RHESSI modulation factor, we derive a measured polarization $\Pi_m = 80 \pm 20\%$.

A number of tests were performed to check that the measured modulation is real. First, we verified that the simulated variation induced by the GRB light curve is accurate by comparing it to an angular distribution of events that were chance coincidences in two detectors. These interactions are nearly simultaneous, but separated by enough time to distinguish them as chance coincidences, not real scattered photons. This distribution should exhibit the same variations owing to the GRB light curve, but no polarization. When we subtracted the simulated distribution from the chance-coincident distribution, we found no evidence for a residual modulation. We have performed a number of independent checks to make sure we do not see modulations from other sources as well. We have verified that extended RHESSI background observations show no sign of modulations. In addition, we have done a preliminary analysis of a strong solar γ-ray flare observed on 23 July 2002, where we see some evidence for a modulation, but corresponding to a polarization $<10\%$. Therefore we feel confident that we have characterized the systematic effects in RHESSI to below the 10% polarization level.

1. Mészáros, P. Theories of gamma-ray bursts. *Annu. Rev. Astron. Astrophys.* **40**, 137–169 (2002).
2. van Paradijs, J., Kouveliotou, C. & Wijers, R. A. M. J. Gamma-ray burst afterglows. *Annu. Rev. Astron. Astrophys.* **38**, 379–425 (2000).
3. Lin, R. P. *et al.* The Reuven Ramaty High Energy Solar Spectroscopic Imager (RHESSI) mission. *Sol. Phys.* (in the press).
4. Novick, R. Stellar and solar X-ray polarimetry. *Space Sci. Rev.* **18**, 389–408 (1975).
5. Lei, F., Dean, A. J. & Hills, A. G. Compton polarimetry in gamma-ray astronomy. *Space Sci. Rev.* **82**, 309–388 (1997).
6. McConnell, M. *et al.* in *Gamma Ray Bursts, 3rd Huntsville Symposium* (eds Kouveliotou, C., Briggs, M. F. & Fishman, G. J.) *AIP Conf. Proc.* **384**, 851–855 (1996).
7. Hurley, K. *et al. GCN Circ.* 1727 (2002).
8. Hurley, K. *et al. GCN Circ.* 1728 (2002).
9. Rybicki, G. B. & Lightman, A. P. *Radiative Processes in Astrophysics* 180–181 (JWS, New York, 1979).
10. Blandford, R. & Eichler, D. Particle acceleration at astrophysical shocks—a theory of cosmic-ray origin. *Phys. Rep.* **154**, 1–75 (1987).
11. Frail, D. A., Waxman, E. & Kulkarni, S. R. A 450 day light curve of the radio afterglow of GRB 970508: fireball calorimetry. *Astrophys. J.* **537**, 191–204 (2000).
12. Freedman, D. & Waxman, E. On the energy of gamma-ray bursts. *Astrophys. J.* **547**, 922–928 (2001).
13. Derishev, E. V., Kocharovsky, V. V. & Kocharovsky, Vl. V. Physical parameters and emission mechanism in gamma-ray bursts. *Astron. Astrophys.* **372**, 1071–1077 (2001).
14. Guetta, D., Spada, M. & Waxman, E. Efficiency and spectrum of internal gamma-ray burst shocks. *Astrophys. J.* **557**, 399–407 (2001).
15. Covino, S. *et al.* GRB 990510: linearly polarized radiation from a fireball. *Astron. Astrophys.* **348**, L1–L4 (1999).
16. Wijers, R. A. M. J. *et al.* Detection of polarization in the afterglow of GRB 990510 with the ESO Very Large Telescope. *Astrophys. J.* **523**, L33–L36 (1999).
17. Rol, E. *et al.* GRB 990712: first indication of polarization variability in a gamma-ray burst afterglow. *Astrophys. J.* **544**, 707–711 (2000).
18. Bersier, D. *et al.* The strongly polarized afterglow of GRB 020405. *Astrophys. J.* **583**, L63–L66 (2003).
19. Waxman, E. γ-ray burst afterglow: confirming the cosmological fireball model. *Astrophys. J.* **489**, L33–L36 (1997).
20. Galama, T. J. *et al.* The effect of magnetic fields on γ-ray bursts inferred from multi-wavelength observations of the burst of 23 January 1999. *Nature* **398**, 394–399 (1999).
21. Medvedev, M. K. & Loab, A. Generation of magnetic fields in the relativistic shock of gamma-ray burst sources. *Astrophys. J.* **526**, 697–706 (1999).
22. Sari, R., Narayan, R. & Piran, T. Cooling timescales and temporal structure of gamma-ray bursts. *Astrophys. J.* **473**, 204–218 (1996).
23. Gruzinov, A. & Waxman, E. Gamma-ray burst afterglow: polarization and analytic light curves. *Astrophys. J.* **511**, 852–861 (1999).
24. Rees, M. J. & Mészáros, P. Unsteady outflow models for cosmological gamma-ray bursts. *Astrophys. J.* **430**, L93–L96 (1994).
25. Spruit, H. C., Daigne, F. & Drenkhahn, G. Large scale magnetic fields and their dissipation in GRB fireballs. *Astron. Astrophys.* **369**, 694–705 (2001).
26. Thompson, C. A model of gamma-ray bursts. *Mon. Not. R. Astron. Soc.* **270**, 480–498 (1994).
27. Mészáros, P. & Rees, M. J. Poynting jets from black holes and cosmological gamma-ray bursts. *Astrophys. J.* **482**, L29–L32 (1997).
28. Blandford, R. D. & Znajek, R. L. Electromagnetic extraction of energy from Kerr black holes. *Mon. Not. R. Astron. Soc.* **179**, 433–456 (1977).
29. Usov, V. V. Millisecond pulsars with extremely strong magnetic fields as a cosmological source of gamma-ray bursts. *Nature* **357**, 472–474 (1992).
30. Gruzinov, A. Gamma-ray burst phenomenology, shock dynamo, and the first magnetic fields. *Astrophys. J.* **563**, L15–L18 (2001).

Experimental entanglement purification of arbitrary unknown states

Jian-Wei Pan, Sara Gasparoni, Rupert Ursin, Gregor Weihs & Anton Zeilinger

Institut für Experimentalphysik, Universität Wien, Boltzmanngasse 5, 1090 Wien, Austria

Distribution of entangled states between distant locations is essential for quantum communication[1–3] over large distances. But owing to unavoidable decoherence in the quantum communication channel, the quality of entangled states generally decreases exponentially with the channel length. Entanglement purification[4,5]—a way to extract a subset of states of high entanglement and high purity from a large set of less entangled states—is thus needed to overcome decoherence. Besides its important application in quantum communication, entanglement purification also plays a crucial role in error correction for quantum computation, because it can significantly increase the quality of logic operations between different qubits[6]. Here we demonstrate entanglement purification for general mixed states of polarization-entangled photons using only linear optics[7]. Typically, one photon pair of fidelity 92% could be obtained from two pairs, each of fidelity 75%. In our experiments, decoherence is overcome to the extent that the technique would achieve tolerable error rates for quantum repeaters in long-distance quantum communication[8]. Our results also imply that the requirement of high-accuracy logic operations in fault-tolerant quantum computation can be considerably relaxed[6].

The resource of quantum entanglement has many important applications in quantum information processing (QIP). In quantum communication, the generation of entanglement between distant

locations is essential for the long-distance realization of quantum cryptography[1], dense coding[2] and quantum teleportation[3]. Meanwhile, quantum information protocols involving entanglement are a very useful tool for fault-tolerant quantum computation[9].

So far, significant experimental progress has been achieved in small-scale realizations of quantum communication[10–14] (up to a few tens of kilometres) and quantum computation[15] (up to a few qubits). However, serious problems occur in bringing QIP to technologically useful scales. One of the most important problems is the unavoidable decoherence due to the coupling between the quantum system and the environment. For instance, because of the noise in the quantum communication channel, the quality of entanglement between two particles is degraded more and more the further they propagate. Yet, the implementation of any of the above quantum communication schemes over large distances requires that two distant parties share highly entangled pairs. It is therefore necessary to overcome the unfavourable decoherence in any realistic large-scale realization of QIP.

One of the main tools used to overcome decoherence in QIP is entanglement purification[4,5]—a method by which one can extract a smaller number of highly entangled pairs out of a large number of less-entangled pairs using only local operations and classical communication. Quantum repeaters[8], based on both entanglement purification[4,5] and entanglement swapping[16], can thus provide an efficient solution to the problems of decoherence and photon loss in long-distance quantum communication[10]. Moreover, a recent study shows that entanglement purification is also important for fault-tolerant quantum computation because it can be used to increase the quality of logic operations between two qubits by several orders of magnitude[6].

Recently, experimental efforts[17–19] have been made to overcome some special decoherence processes using the ideas of local filtering
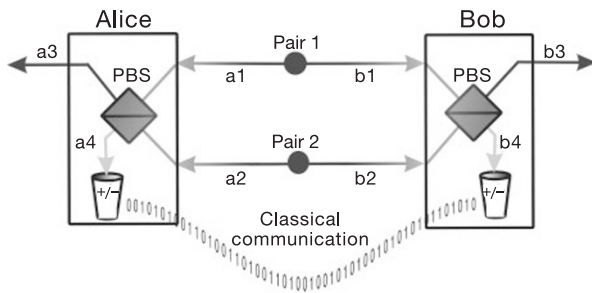

Figure 1 Schematic drawing showing the principle of entanglement purification using linear optics. We start with two less entangled pairs shared by Alice and Bob who superpose their photons on a polarizing beam splitter (PBS). Alice and Bob keep only those cases where there is exactly one photon in each output mode ('four-mode cases'). They perform a polarization measurement in the $\pm$ basis in modes a4 and b4, where $|+\rangle = (1/\sqrt{2})(|H\rangle + |V\rangle)$ and $|-\rangle = (1/\sqrt{2})(|H\rangle - |V\rangle)$. Depending on the results, Alice performs a specific operation on the photon in mode a3. After this procedure, the remaining pair in modes a3 and b3 will have a higher degree of entanglement than the two original pairs. To explain the protocol in detail, we consider the case where both pairs are in the state $|\Phi^+\rangle_{ab}$, which occurs with a probability of F^2 in our example. For the state $|\Phi^+\rangle_{a1b1} \cdot |\Phi^+\rangle_{a2b2}$, considering only those cases for which one, and only one, photon is finally found in modes a4 and b4 one obtains the state $(1/2)(|H\rangle_{a3}|H\rangle_{a4}|H\rangle_{b3}|H\rangle_{b4} + |V\rangle_{a3}|V\rangle_{a4}|V\rangle_{b3}|V\rangle_{b4})$. This shows that the probability for a four-mode case is 50%. Alice and Bob can then generate maximal two-photon entanglement between the output modes a3 and b3 out of the four-photon entanglement by performing polarization measurements on each of the two photons at a4 and b4 in the $\pm$ basis and comparing their results. If the measurement results at a4 and b4 are the same—that is, $|+\rangle|+\rangle$ or $|-\rangle|-\rangle$—then the remaining two photons at a3 and b3 are left in the state $|\Phi^+\rangle_{a3b3}$. If the results are opposite, namely $|+\rangle|-\rangle$ or $|-\rangle|+\rangle$, then the remaining two photons are left in the state $|\Phi^-\rangle_{a3b3}$. In the second case, Alice can simply apply a local phase-flip operation on her remaining photon to convert the state $|\Phi^-\rangle_{a3b3}$ back to $|\Phi^+\rangle_{a3b3}$.

and entanglement concentration[20]. However, the implementation of a general entanglement purification scheme[4,5] that works for arbitrary unknown decoherence processes remains an experimental challenge. The main practical drawback of the original purification scheme[4,5] is that it requires the CNOT operation. However, there is at present no implementation of CNOT gates between independent qubits that could be used for purification in the context of long-distance quantum communication. This is because the tolerable error rates of the CNOT operation must not exceed a few per cent[8], which is far beyond what is experimentally possible at present. Fortunately, it was shown recently that this problem can be overcome by a general purification method that requires only linear optical elements[7].

We now briefly explain the linear optical purification scheme[7] (shown in Fig. 1) by discussing a specific example. Suppose that two distant parties, Alice and Bob, need to share photon pairs in the polarization entangled state $|\Phi^+\rangle_{ab}$ for a certain quantum communication task. We use the four usual Bell states:

$$|\Phi^\pm\rangle_{ab} = \frac{1}{\sqrt{2}}(|H\rangle_a|H\rangle_b \pm |V\rangle_a|V\rangle_b)$$

$$|\Psi^\pm\rangle_{ab} = \frac{1}{\sqrt{2}}(|H\rangle_a|V\rangle_b \pm |V\rangle_a|H\rangle_b)$$

$$(1)$$

where H (or V) denotes horizontal (or vertical) linear polarization, and subscripts a (or b) indicates the particle at Alice's (or Bob's) locations. Suppose further that, owing to noise in the quantum communication channel, the pairs they share before purification are in the mixed state:

$$\rho_{ab} = F|\Phi^+\rangle_{ab}\langle\Phi^+| + (1 - F)|\Psi^-\rangle_{ab}\langle\Psi^-| \qquad (2)$$

where $|\Psi^-\rangle_{ab}$ is an unwanted admixture. Without loss of generality, we choose this specific form of ρ_{ab} just for the convenience of discussion. The entanglement fidelity with respect to $|\Phi^+\rangle_{ab}$ is then given by $F = \langle\Phi^+|\rho_{ab}|\Phi^+\rangle$.

Alice and Bob start by choosing two pairs from the ensemble ρ_{ab}. Each of them then superimposes their photons on a polarizing beam splitter (PBS). The PBS with two input modes and two output modes transmits horizontal and reflects vertical polarization. An essential step in our purification scheme is to select those cases where there is exactly one photon in each of the four spatial output modes, which we refer to as 'four-mode cases'.

From equation (2) it follows that the original state of the two pairs can be seen as a probabilistic mixture of four cases: with a probability of F^2, pairs 1 and 2 are in the state $|\Phi^+\rangle_{a1b1} \cdot |\Phi^+\rangle_{a2b2}$, with equal probabilities of $F(1 - F)$ in the states $|\Psi^-\rangle_{a1b1} \cdot |\Phi^+\rangle_{a2b2}$ and $|\Phi^+\rangle_{a1b1} \cdot |\Psi^-\rangle_{a2b2}$, and with a probability of $(1 - F)^2$ in $|\Psi^-\rangle_{a1b1} \cdot |\Psi^-\rangle_{a2b2}$.

It is easy to see that the cross combinations $|\Psi^-\rangle_{a1b1} \cdot |\Phi^+\rangle_{a2b2}$ and $|\Phi^+\rangle_{a1b1} \cdot |\Psi^-\rangle_{a2b2}$ never lead to four-mode cases, because in these two cases only three photons always have equal polarization. Thus, by selecting only four-mode cases one can eliminate the cases that have one single bit-flip error.

Consider now the other two combinations $|\Phi^+\rangle_{a1b1} \cdot |\Phi^+\rangle_{a2b2}$ and $|\Psi^-\rangle_{a1b1} \cdot |\Psi^-\rangle_{a2b2}$. Let us first discuss the $|\Phi^+\rangle_{a1b1} \cdot |\Phi^+\rangle_{a2b2}$ case. In Fig. 1 we show that following our protocol Alice and Bob will get the state $|\Phi^+\rangle_{a3b3}$ whenever there is exactly one photon in each output mode, that is, with a probability of 50%. In the $|\Psi^-\rangle_{a1b1} \cdot |\Psi^-\rangle_{a2b2}$ case, following the same procedure, Alice and Bob will project the remaining two photons a3 and b3 into the state $|\Psi^+\rangle_{a3b3}$ with a probability of 50%.

Because the probabilities for $|\Phi^+\rangle_{a1b1} \cdot |\Phi^+\rangle_{a2b2}$ and $|\Psi^-\rangle_{a1b1} \cdot |\Psi^-\rangle_{a2b2}$ are F^2 and $(1 - F)^2$ respectively, after performing the purification procedure Alice and Bob will obtain the state $|\Phi^+\rangle_{a3b3}$ with a probability of $F^2/2$ and the state $|\Psi^+\rangle_{a3b3}$ with a probability of $(1 - F)^2/2$. By applying our procedure, they can thus

create a new ensemble described by the density operator

$$\rho'_{ab} = F'|\Phi^+\rangle_{ab}\langle\Phi^+| + (1-F')|\Psi^-\rangle_{ab}\langle\Psi^-| \quad (3)$$

with a larger fraction of $F' = F^2/[F^2 + (1-F)^2] > F$ (for $F > 1/2$) of pairs in the desired state $|\Phi^+\rangle_{ab}$ than before the purification.

Until now, it seems that we have only discussed a rather special example, that is, how to eliminate single bit-flip errors. However, it has been shown[4,7] that with twirling (that is, rotating bases between individual purification steps or randomly choosing bases), the same method would also apply to the general mixed states ρ_{ab}, provided that they contain a sufficiently large fraction $F > 1/2$ of photon pairs in a maximally entangled state, $|\Phi^+\rangle_{ab}$ in our case. In short, this can be understood as follows. Using our purification method, one can first purify away single bit-flip errors. Phase errors can then be transformed into bit-flip errors by a 45° polarization rotation and treated in a subsequent purification step. Therefore, to demonstrate the generality of our scheme, it is sufficient to verify the purification

effect for the mixed state described in equation (2).

To demonstrate the purification scheme experimentally using only linear optical elements, we need to process two photon pairs which are in the mixed state (2). A schematic drawing of our experimental set-up is shown in Fig. 2. In our experiment, the required photon pairs are produced by parametric down-conversion from an ultraviolet pulsed laser in a beta barium borate (BBO) crystal[21]. We then interfere the two photons at Alice's (or Bob's) side in the pair a1–a2 (or b1–b2) at a PBS by making them indistinguishable. To achieve this indistinguishability, several methods have been used to guarantee that the photons at the same PBS have a perfect spatial and temporal overlap[22] (see Fig. 3a and Methods section). After the four photons' passage through the two PBS, the
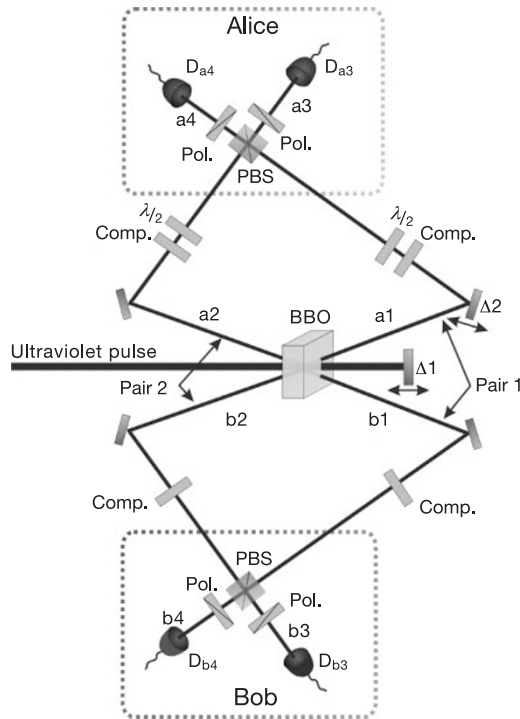

Figure 2 Experimental set-up for entanglement purification. A pulse of ultraviolet light passes through a BBO crystal twice to produce two polarization-entangled photon pairs, that is, pair 1 in a1–b1 and pair 2 in a2–b2. The ultraviolet laser with a central wavelength of 394 nm has a pulse duration of 200 fs and a repetition rate of 76 MHz. Four compensators (Comp.) are used to offset the birefringent effect caused by the BBO crystal during parametric down-conversion. In the experiment, with an average pump power of 500 mW, we are able to observe about 1.7×10^4 entangled pairs per second. The two photon pairs are originally prepared in the state $|\Phi^+\rangle_{ab}$, with a high signal-to-noise ratio of 30:1 in the ± basis. One member of each pair (the photons a1 and a2) is further sent through a half-wave plate ($\lambda/2$), whose angle is randomly set at either $+\delta$ or $-\delta$, to prepare the mixed state (2). Here, in order for the two pairs a1–b1 and a2–b2 to have roughly the same twofold coincidence, we have carefully chosen four detectors which have almost-equal detection efficiency. This arrangement ensures that the difference in twofold coincidence between pair a1–b1 and pair a2–b2 is less than 5% in all measurements. These features allow us to perform a precise analysis on the accuracy of our purification protocol. We then send the two pairs through the corresponding PBS to perform entanglement purification. By adjusting the positions of the delay mirrors Δ1 and Δ2, we can achieve simultaneous arrival of the photons at their respective PBS. Detecting exactly one photon in each of the four outputs (a3, a4, b3 and b4) behind a 45° polarizer (Pol.), one can verify the success of the purification scheme.
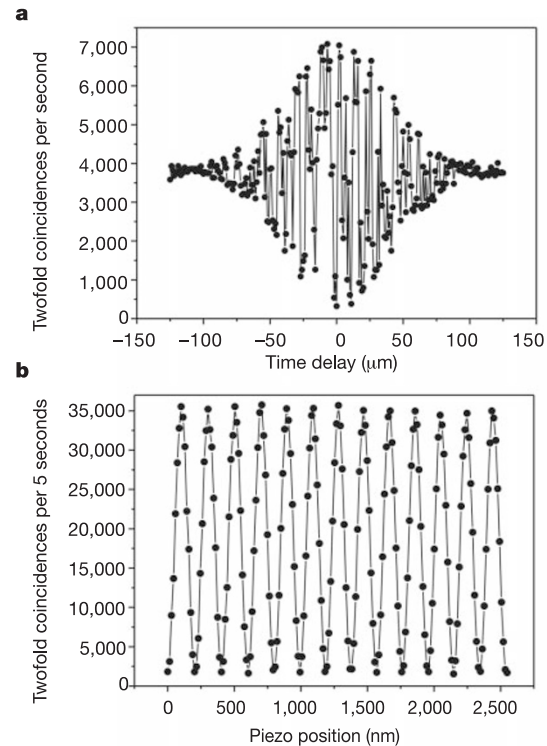

Figure 3 Experimental results showing the procedures to achieve perfect temporal overlap and to adjust the phase $\phi_4 = 0$. **a**, After roughly achieving the temporal overlap of modes b1 and b2, and of modes a1 and a2, we measure the twofold coincidence between the output modes a4 and b4 behind 45° polarizers, by scanning the position of Δ1 with a step size of 1 μm. The envelope of the observed twofold coincidence varies indicating the visibility of the two-photon coherence. Outside the coherent region, $|H\rangle_{a4}|H\rangle_{b4}$ and $|V\rangle_{a4}|V\rangle_{b4}$ are distinguishable, so no interference occurs. Inside the coherent region, the best visibility is obtained at the position where perfect temporal overlap is achieved. We perform fine adjustment of the position of Δ2 and repeat the scanning of Δ1 until the best visibility is obtained. **b**, We use a piezo translation stage to move the mirror Δ1 to perform a fine scan around the region of zero delay, that is, around the centre of the envelope. By setting the piezo system to a position where we observe maximum twofold coincidence of a4–b4, ϕ_2 thus equals 0 and so does ϕ_4. Note that in the experiment we also insert one 45° polarizer into each of the outputs a3 and b3 and measure their twofold coincidence. Another sine curve is observed (not shown). Usually the twofold coincidences of a4–b4 and of a3–b3 do not vary synchronously as we move the piezo system. This is caused by the birefringent effect, that is, the H and V polarizations of a photon accumulate a different phase during its passage through the PBS. This ultimately implies that the $|H\rangle|H\rangle$ and $|V\rangle|V\rangle$ components in a3–b3 acquire a relative phase ϕ'_2, which is different from ϕ_2. Experimentally, we introduce an additional birefringent element to compensate for the above effect. After this compensation, the two curves exhibit perfect synchronization, that is, $\phi_2 = \phi'_2$.

 419

two photons in the mode pair a3–b3 have a higher probability to be in the desired state $|\Phi^+\rangle_{ab}$ if we detect one and only one photon polarized along the $\pm$ basis in each of the modes a4 and b4. Here we note that, owing to the absence of single-photon detectors, it is for the time being necessary also to detect the purified photons in a3 and b3 to ensure a fourfold event.

Thus far, we have considered only the ideal case, where there is at most one pair of photons in each of the input modes a1–b1 and a2–b2. However, with a probability of the same order of magnitude, two photon pairs will be emitted into the same mode pair because parametric down-conversion is a spontaneous process. This case could also result in four-mode cases in the real experiment. Specifically, if the two photon pairs are both in the mode pair a1–b1, we will then sometimes obtain a four-mode contribution that is in the state $|V\rangle_{a3}|H\rangle_{a4}|V\rangle_{b3}|H\rangle_{b4}$; and, if the two photon pairs are both in a2–b2, we will sometimes obtain the four-mode contribution $|H\rangle_{a3}|V\rangle_{a4}|H\rangle_{b3}|V\rangle_{b4}$.

As pointed out in ref. 7, if the position of the reflection mirror $\Delta1$ is fixed and the amplitudes of these two four-mode contributions arrive at the two PBS simultaneously, then the two amplitudes will have a fixed relative phase (denoted by ϕ_4) and thus be in a coherent superposition $|H\rangle_{a3}|V\rangle_{a4}|H\rangle_{b3}|V\rangle_{b4} + e^{i\phi_4}|V\rangle_{a3}|H\rangle_{a4}|V\rangle_{b3}|H\rangle_{b4}$. Interestingly, adjusting the position of $\Delta1$ such that $\phi_4 = 0$ and further performing a polarization measurement in the mode pair a4–b4 in the $\pm$ basis, in our purification protocol the two remaining photons in a3–b3 will always be converted into the state $|\Phi^+\rangle_{ab}$, which is exactly the desired maximally entangled state. This implies that the presence of double pair emission into the same mode pair in no way prevents us from carrying out the purification protocol, but rather makes the scheme more efficient (see ref. 23 for a detailed analysis).

Having achieved perfect spatial and temporal overlap and having fixed the relative phase ϕ_4 to zero (see Fig. 3 and the Methods section), we then experimentally demonstrated entanglement purification. In the first purification experiment, we prepare ρ_{ab} in the mixed state of equation (2) with an entanglement fidelity of $F = 0.75$, by randomly setting the half-wave plate axis to be oriented at $\pm14°$ (that is, $\delta = 14°$). This implies that with a probability of 75%, the photon pairs will be in the desired state $|\Phi^+\rangle_{ab}$, and with a probability of 25% in the unwanted state $|\Psi^-\rangle_{ab}$. This is confirmed by the experimentally measured fractions both in the H/V and in the $\pm$ bases for the original mixed state, as shown in Fig. 4a and b respectively.

After purification, provided there is one and only one single photon detection in each of the modes a4 and b4 along the $\pm$ basis, we expect the two remaining photons in the modes a3 and b3 to acquire a high quality of entanglement. To verify this, we first measure the fractions in the H/V basis for the purified mixed state of a3–b3. The integration time is about 0.5 h for each of the four components HH, HV, VH and VV, and we collect about 700 fourfold coincidences for the maximum (HH or VV) and 60 for the minimum (HV or VH). The experimental results are shown in Fig. 4c. Compared with Fig. 4a, the fractions in Fig. 4c clearly confirm the significant improvement in the purity of the mixed state in the H/V basis.

Showing the improvement of purity in the H/V basis alone is a necessary but not a sufficient experimental criterion for the verification of entanglement purification, because the result in Fig. 4c is, in principle, both compatible with ρ'_{ab} (highly entangled) and with a statistical mixture of HH, HV, VH and HH (no entanglement at all). Thus, to exclude the latter case, we also measure the fractions of the purified state in the $\pm$ basis. Together with Fig. 4b, the results in Fig. 4d confirm the enhancement of entanglement well. Figure 4c and d show the significant improvement in entanglement fidelity, thus demonstrating the success of entanglement purification. The fidelity F' of the purified sub-ensemble is now about 0.92 ± 0.01.

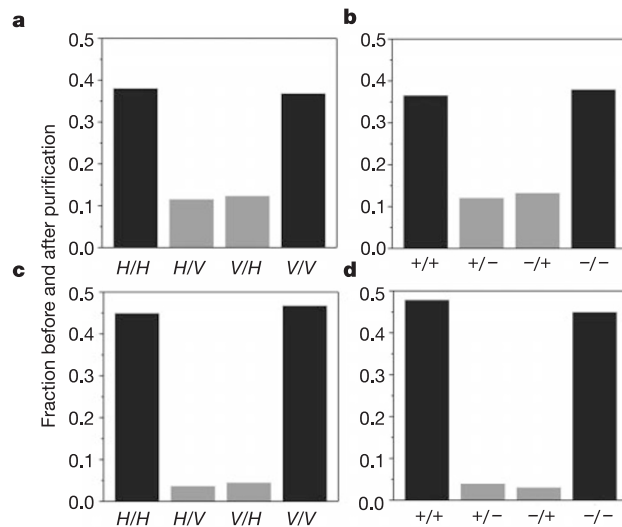As a further demonstration, in a second experiment we also

Figure 4 Experimental results. **a** and **b** show the experimentally measured fractions both in the H/V and in the $\pm$ bases for the original mixed state. **c** and **d** show the measured fractions of the purified state in the modes a3 and b3 both in the H/V and in the $\pm$ bases. Compared with the fractions in **a** and **b**, our experimental results shown in **c** and **d** together confirm the success of entanglement purification through the observed reduction of the fractions of the mixed (H/V and $\pm$) cases.

performed entanglement purification for the mixed state with fidelity parameter $F = 0.80$. After performing purification, the observed entanglement fidelity for the sub-ensemble in the modes a3 and b3 is about 0.94 ± 0.01. This again verifies our purification scheme. It is worth noting that in both experiments, the visibilities of the original mixed states are 50% and 60%, respectively. However, after one-step purification the visibilities of the new ensembles are 84% and 88%: these are both well above the threshold above which Bell's inequality is violated, and are thus sufficient to ensure secure quantum communication.

We now briefly analyse the experimental accuracy of our purification method. As mentioned above, in our experiment we have two cases which contribute to the fourfold coincidence, that is, the case where there is one and only one entangled pair in each of the mode pairs a1–b1 and a2–b2, and the case where both entangled pairs are in the same mode pair. Consider an ensemble that is initially prepared in the mixed state (2). Thus, after purification the first case will result in a new mixed state that is described by equation (3), whereas the second case will always result in the desired entangled state $|\Phi^+\rangle_{ab}$. Note that these two cases contribute to the fourfold coincidence with the same probability. To determine the accuracy of our method, we first measure the entanglement fidelity of the pairs in a3–b3 (conditioned on a $|+\rangle|+\rangle$ coincidence detection in a4–b4) before introducing the channel noise. The observed fidelity is about 0.95, which represents the entanglement quality of the pairs in a3–b3 contributed from the double pair emission.

After taking into account this imperfection and subtracting the contribution of the double pair emission, we can calculate the purification accuracy of the first case. We consider, for example, the first experiment, in which the original ratio between the desired state and the unwanted state is 3:1. After purification, the final ratio of the first case is found to be about 8:1, which is in excellent agreement with the theoretical value 9:1 (refer to the text after equation (3)). From the obtained final ratio we can further estimate the accuracy of local operations at the PBS, which is better than 98%, or equivalently an error probability of at most 2%.

In the present experiment, we report the first demonstration of a general entanglement purification protocol. Entanglement purifi-

cation with high accuracy is important not only for quantum communication, but also for quantum computation. On the one hand, together with our recent experimental realization of high-fidelity teleportation[14], the present experiment implies that the threshold of tolerable error rates in quantum repeaters can be achieved[8]. In that sense, we claim that our experimental results demonstrate for the first time the feasibility of overcoming the decoherence in scalable quantum communication. This opens up the possibility of realistic quantum communication over large distances. On the other hand, with the help of entanglement purification, the strict accuracy requirements of the gate operations for fault-tolerant quantum computation can also be significantly reduced[6].

The methods developed in our purification experiment have many useful applications in the field of linear optics QIP and in experimental tests of quantum nonlocality. It was noted recently that, while our set-up directly enables an implementation of a non-destructive C-NOT gate with a success probability of 25% (ref. 24), a slight modification of the set-up also provides a simple way to implement a nonlinear sign gate[25]—a fundamental element in linear optics quantum computation[26]. Furthermore, our methods of achieving perfect spatial-temporal overlap and phase stabilization provide the necessary techniques for experimental investigations of schemes in quantum communication with linear optics and atomic ensembles[27].

Meanwhile, although the requirement of phase stabilization appears to be a drawback in long-distance quantum communication, this problem can be solved in our purification scheme by using entangled photon pairs produced with quantum dots[28] instead of by parametric down-conversion. Finally, the two-photon four-dimensional entanglement exploited in the experiment also enables us to perform an experimental test of 'all versus nothing' quantum nonlocality for two particles[29] and high-efficiency entanglement-assisted quantum cryptography[30]. □

Methods

Making two independent photons indistinguishable

To make two independent photons indistinguishable, one has to guarantee that the two photons have good spatial and temporal overlap at the PBS. To achieve this, the two outputs of the PBS are spectrally filtered (3-nm bandwidth) and monitored by fibre-coupled detectors (either D_{a3} and D_{a4} or D_{b3} and D_{b4}). While the single-mode fibre couplers act as spatial filters to guarantee good mode overlap of the detected photons, the narrow bandwidth filters stretch the coherence time to about 700 fs, substantially larger than the pump-pulse duration. The filtering process effectively erases any possibility of distinguishing the two photons according to their arrival time and therefore leads to interference[22].

To meet the condition of temporal overlap, the two photons at the same location (Alice's or Bob's) must arrive at their PBS simultaneously. To achieve this, we first move $\Delta 1$ in small steps to search for the position (denoted by p_b) where the two photons in b1 and b2 have the same arrival time. Then we insert one 45° polarizer into each of the modes b1 and b2 and observe the two-photon Hong–Ou–Mandel (HOM) dip after the PBS by performing polarization measurements in both modes b3 and b4 in the ± basis. The maximum interference occurs at the region of zero delay, that is, at the centre of the HOM dip. In a similar manner, we can find the position of $\Delta 1$ (denoted by p_a) where the two photons in a1 and a2 have the same arrival time. Fixing the position of $\Delta 1$ at p_b and moving the mirror $\Delta 2$ by a distance $p_b - p_a$, we can thus roughly achieve temporal overlap. After this preliminary alignment, we take away the polarizers in the input modes. Because the polarizers have slightly different time delays, it is necessary to further improve the temporal overlap both of the mode pair a1–a2 and of the mode pair b1–b2.

Here we exploit a two-photon four-dimensional entangled state[23,29]. This corresponds to the case where one and only one entangled pair is created after the pump pulse has passed through the BBO crystal twice, that is, the entangled photon pair is emitted into a superposition of the mode pairs a1–b1 and a2–b2. Thus, before the photon pair passes through the noisy channel the two-photon four-dimensional entangled state can be written as $(|H\rangle_a|H\rangle_b + |V\rangle_a|V\rangle_b)(|a1\rangle|b1\rangle + e^{i\phi_2}|a2\rangle|b2\rangle)$, where $|a1\rangle|b1\rangle$ and $|a2\rangle|b2\rangle$ denote the spatial wavefunctions of the photon pair, and their relative phase is ϕ_2 determined by the position of the reflection mirror $\Delta 1$. Furthermore, if the amplitudes of the spatial modes a1–a2 and b1–b2 arrive at their own PBS simultaneously, then after the four-dimensional entangled state passes through the PBS, the two photons in a4–b4 will be in the polarization state $|H\rangle_{a4}|H\rangle_{b4} + e^{i\phi_2}|V\rangle_{a4}|V\rangle_{b4}$. By observing two-photon interference fringes between the modes a4 and b4, we can then achieve perfect temporal overlap (see Fig. 3a for details).

Achieving a fixed phase of $\phi_4 = 0$

Usually, one can find the right position of $\Delta 1$, that is, $\phi_4 = 0$, by measuring the fourfold polarization correlation in the ± basis. However, in the real experiment, owing to the low fourfold coincidence rate, which was about five per second on average, it is very difficult to find the correct position of $\Delta 1$ in this way. To achieve $\phi_4 = 0$, here we again exploit the two-photon four-dimensional entangled state. Because the two relative phases ϕ_4 and ϕ_2 satisfy the relation $\phi_4 = 2\phi_2$, it follows that if $\phi_2 = 0$, then $\phi_4 = 0$ (see ref. 23). Indeed, we can then determine the relative phase by measuring, for example, the polarization correlation for the two photons in the mode pair a4–b4. Therefore, by inserting a 45° polarizer in each of the output modes a4 and b4 and scanning the reflection mirror $\Delta 1$ we can observe a two-photon interference sine curve in the mode pair a4–b4. Setting $\Delta 1$ to a position where a maximum coincidence rate for $|+\rangle|+\rangle$ is obtained, we can fix both phases ϕ_4 and ϕ_2 to 0.

To have a fixed phase of $\phi_4 = 0$, phase stabilization is required throughout the whole measurement. To achieve this, we built the set-up on a thick aluminium platform to avoid sound resonance, used feedback air-conditioning to avoid thermal expansion of the interferometer, and built a plastic housing around the set-up to avoid air flow. At the same time, we also use the twofold coincidence of a4–b4 as a phase monitor. In this way, we are able to keep the phase stable for several hours. We emphasize that, as opposed to the earlier multi-photon experiments, here we require interferometric precision and stability where the scale is the wavelength and is therefore much smaller than coherence stability. This was particularly difficult and challenging to achieve.

1. Ekert, A. Quantum cryptography based on Bell's theorem. *Phys. Rev. Lett.* **67**, 661–663 (1991).
2. Bennett, C. H. & Wiesner, S. J. Communication via one- and two-particle operators on Einstein-Podolsky-Rosen states. *Phys. Rev. Lett.* **69**, 2881–2884 (1992).
3. Bennett, C. H. *et al.* Teleporting an unknown quantum state via dual classical and Einstein-Podolsky-Rosen channels. *Phys. Rev. Lett.* **83**, 3081–3084 (1993).
4. Bennett, C. H. *et al.* Purification of noisy entanglement, and faithful teleportation via noisy channels. *Phys. Rev. Lett.* **76**, 722–725 (1996).
5. Deutsch, D. *et al.* Quantum privacy amplification and the security of quantum cryptography over noisy channels. *Phys. Rev. Lett.* **77**, 2818–2821 (1996).
6. Duer, W. & Briegel, H.-J. Entanglement purification for quantum computation. *Phys. Rev. Lett.* **90**, 067901 (2003).
7. Pan, J.-W., Simon, C., Brukner, C. & Zeilinger, A. Entanglement purification for quantum communication. *Nature* **410**, 1067–1070 (2001).
8. Briegel, H.-J., Duer, W., Cirac, J. I. & Zoller, P. Quantum repeaters: The role of imperfect local operations in quantum communication. *Phys. Rev. Lett.* **81**, 5932–5935 (1998).
9. Gottesman, D. & Chuang, I. L. Demonstrating the viability of universal quantum computation using teleportation and single-qubit operations. *Nature* **402**, 390–393 (1999).
10. Gisin, N., Ribordy, G., Tittel, W. & Zbinden, H. Quantum cryptography. *Rev. Mod. Phys.* **74**, 145–195 (2002).
11. Mattle, K., Weinfurter, H., Kwiat, P. G. & Zeilinger, A. Dense coding in experimental quantum communication. *Phys. Rev. Lett.* **76**, 4656–4659 (1996).
12. Bouwmeester, D. *et al.* Experimental quantum teleportation. *Nature* **390**, 575–579 (1997).
13. Marcikic, I., de Riedmatten, H., Tittel, W., Zbinden, H. & Gisin, N. Long-distance teleportation of qubits at telecommunication wavelengths. *Nature* **421**, 509–513 (2003).
14. Pan, J.-W., Gasparoni, S., Aspelmeyer, M., Jennewein, T. & Zeilinger, A. Experimental realization of freely propagating teleported qubits. *Nature* **421**, 721–725 (2003).
15. Jones, J. Quantum computing: Putting it into practice. *Nature* **421**, 28–29 (2003).
16. Zukowski, M., Zeilinger, A., Horne, M. A. & Ekert, A. "Event-ready-detectors" Bell experiment via entanglement swapping. *Phys. Rev. Lett.* **71**, 4287–4290 (1993).
17. Kwiat, P. G., Barraza-Lopez, S., Stefanov, A. & Gisin, N. Experimental entanglement distillation and 'hidden' non-locality. *Nature* **409**, 1014–1017 (2001).
18. Yamamoto, T., Koashi, M., Ozdemir, S. K. & Imoto, N. Experimental extraction of an entangled photon pair from two identically decohered pairs. *Nature* **421**, 343–346 (2003).
19. Zhao, Z., Yang, T., Chen, Y.-A., Zhang, A.-N. & Pan, J.-W. Experimental realization of entanglement concentration and a quantum repeater. *Phys. Rev. Lett.* (in the press); preprint available at ⟨http://xxx.lanl.gov/quant-ph/0211075⟩ (2003).
20. Bennett, C. H., Bernstein, H. J., Popescu, S. & Schumacher, B. Concentrating partial entanglement by local operations. *Phys. Rev. A* **53**, 2046–2052 (1996).
21. Kwiat, P. G. *et al.* New high intensity soure of polarization-entangled photon. *Phys. Rev. Lett.* **75**, 4337–4341 (1995).
22. Zukowski, M., Zeilinger, A. & Weinfurter, H. Entangling photons radiated by independent pulsed source. *Ann. NY Acad. Sci.* **755**, 91–102 (1995).
23. Simon, C. & Pan, J.-W. Polarization entanglement purification using spatial entanglement. *Phys. Rev. Lett.* **89**, 257901 (2002).
24. Pittman, T. B., Jacobs, B. C. & Franson, J. D. Demonstration of nondeterministic quantum logic operations using linear optical elements. *Phys. Rev. Lett.* **88**, 257902 (2002).
25. Rudolph, T. & Pan, J.-W. A simple gate for linear optics quantum computing. Preprint available at ⟨http://xxx.lanl.gov/quant-ph/0108056⟩ (2001).
26. Knill, E., Laflamme, R. & Milburn, G. J. A scheme for efficient quantum computation with linear optics. *Nature* **409**, 46–52 (2001).
27. Duan, L.-M., Lukin, M. D., Cirac, J. I. & Zoller, P. Long-distance quantum communication with atomic ensembles and linear optics. *Nature* **414**, 413–418 (2001).
28. Santori, C., Fattal, D., Vuckovic, J., Solomon, G. S. & Yamamoto, Y. Indistinguishable photons from a single-photon device. *Nature* **419**, 594–596 (2001).
29. Chen, Z.-B., Pan, J.-W., Zhang, Y.-D., Brukner, C. & Zeilinger, A. All-versus-nothing violation of local realism for two entangled photons. *Phys. Rev. Lett.* **90**, 160408 (2003).
30. Zhao, Z., Yang, T., Chen, Z.-B., Du, J.-F. & Pan, J.-W. Deterministic and highly efficient quantum cryptography with entangled photon pairs. Preprint available at ⟨http://xxx.lanl.gov/quant-ph/0211098⟩ (2002).

421

letters to nature

....

Real-time detection of electron tunnelling in a quantum dot

Wei Lu*†, **Zhongqing Ji***, **Loren Pfeiffer**‡, **K. W. West**‡ & **A. J. Rimberg***§

* *Department of Physics and Astronomy,* § *Department of Electrical and Computer Engineering, Rice University, Houston, Texas 77005, USA*
‡ *Bell Laboratories, Lucent Technologies, Inc., Murray Hill, New Jersey 07974, USA*

....

Nanostructures in which strong (Coulomb) interactions exist between electrons are predicted to exhibit temporal electronic correlations[1]. Although there is ample experimental evidence that such correlations exist[2], electron dynamics in engineered nanostructures have been observed directly only on long time-scales[3]. The faster dynamics associated with electrical currents or charge fluctuations[4] are usually inferred from direct (or quasi-direct) current measurements. Recently, interest in electron dynamics has risen, in part owing to the realization that additional information about electronic interactions can be found in the shot noise[5] or higher statistical moments[6,7] of a direct current. Furthermore, interest in quantum computation has stimulated investigation of quantum bit (qubit) readout techniques[8,9], which for many condensed-matter systems ultimately reduce to single-shot measurements of individual electronic charges. Here we report real-time observation of individual electron tunnelling events in a quantum dot using an integrated radio-frequency single-electron transistor[10,11]. We use electron counting to measure directly the quantum dot's tunnelling rate and the occupational probabilities of its charge state. Our results provide evidence in favour of long (10 μs or more) inelastic scattering times in nearly isolated dots.

Real-time detection of individual electrons is a formidable task: the electronic charge is small, and typical timescales for electronic dynamics are short, ranging from picoseconds to microseconds. We therefore require a detector with both a low charge noise of $\delta q \approx 1 \times 10^{-5} e\,\mathrm{Hz}^{-1/2}$ and a fast response time of roughly a microsecond or less. The recently developed radio-frequency single-electron transistor (RF-SET)[10,11] satisfies both requirements, and we use such a device as the basis of our detection scheme. Our system of choice for investigation of charge dynamics is a quantum dot (QD), a small conducting region in a semiconductor that contains a few to a few thousand electrons. Sufficiently small QDs contain well-defined energy levels, and are often referred to as artificial atoms. A QD is typically connected to macroscopic leads by tunnel barriers, allowing access to its internal state. Importantly, these tunnel barriers and other dot properties can be adjusted to allow studies of electron dynamics.

We have performed measurements on three different samples, each consisting of a QD and an integrated RF-SET detector. All three showed similar behaviour, and here we present results from two of them (S1 and S2). When the QD is formed by application of gate voltages (Fig. 1a), it contains a well-defined number of electrons N; at low temperatures and bias voltages N can change only by ±1. The capacitive SET–QD coupling ensures that such a change shifts the polarization charge Q_{SET} of the SET island by some fraction of an electronic charge e; typically $\Delta Q_{SET} \approx (0.1–0.2)e$ for our samples. The shift ΔQ_{SET} changes the differential resistance R_d of the SET, which in turn allows SET-based electrometry[12,13]. In radio-frequency (r.f.) operation, changes in R_d modulate the amplitude of a carrier wave reflected from a resonant circuit containing the SET (Fig. 1b). Demodulating the carrier wave recovers the modulating signal (Fig. 1c), forming the basis for real-time measurements of the QD charge Q_{QD}.

When the dot is sufficiently isolated from the surrounding two-dimensional electron gas (2DEG), we observe switching behaviour in the RF-SET output (Fig. 1d) reminiscent of random telegraph signals (RTSs) associated with engineered[3] or naturally occurring[14,15] charge traps. We have taken pains to ensure that the RTS we observe is due to individual electron tunnelling events on the QD. The size of the RTS for S1 as determined by comparison to a $0.05e$ r.m.s. sine wave (Fig. 1c and d) corresponds to $\Delta Q_{SET} \approx 0.1e$,
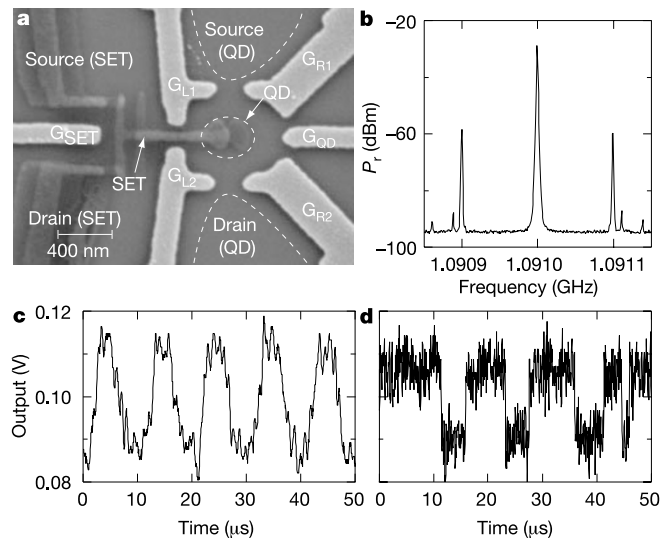

Figure 1 Characterization of RF-SET response. **a**, Electron micrograph of the sample design for S1. We begin with a GaAs/AlGaAs heterostructure containing a 2DEG located 190 nm below the sample surface. At 4 K, the 2DEG sheet density is $1.3 \times 10^{11}\,\mathrm{cm}^{-2}$ and its mobility is $4.1 \times 10^6\,\mathrm{cm}^2\,\mathrm{V}^{-1}\,\mathrm{s}^{-1}$. The SET consists of a small Al island connected to a source and drain through small tunnel barriers (total resistance 15 kΩ) formed by a thin AlO$_x$ layer and has a charging energy $E_{C_{SET}} = e^2/2C_{SET} \approx 162\,\mu\mathrm{eV}$ where C_{SET} is the total SET capacitance. The SET is superconducting for all measurements, which were made in a dilution refrigerator at its base temperature of 15 mK. The dot is formed by applying a negative voltage to the Au gates G$_{L1}$, G$_{L2}$, G$_{R1}$, G$_{R2}$ and G$_{QD}$, leaving a small pool of electrons at their centre. The SET island extends between G$_{L1}$ and G$_{L2}$ to lie above the QD and maximize sensitivity to its charge. Gate G$_{SET}$ is used to adjust the SET offset charge Q_{SET}. The QD can be coupled by tunnel barriers to its own source and drain, or isolated completely from them. The dot has an estimated area $A \approx 200\,\mathrm{nm} \times 300\,\mathrm{nm}$ and contains roughly 80 electrons with an average level spacing $\Delta \approx 1/Ag_{2D} \approx 60\,\mu\mathrm{eV}$; here $g_{2D} = m^*/\pi \hbar^2$ is the two-dimensional density of states, and m^* is the effective mass of GaAs. **b**, Power spectral density P_r of a reflected carrier wave at 1.091 GHz for which Q_{SET} is modulated by a 100-kHz, $0.05e$ r.m.s. sine wave. For S1, a d.c. SET bias of 500 μV and r.f. amplitude of 87 μV r.m.s. gave a charge sensitivity of $\delta q \approx 2.4 \times 10^{-5} e\,\mathrm{Hz}^{-1/2}$ that was relatively insensitive to Q_{SET}. **c**, Demodulated signal for the reflected wave in **b**, passed through a low-pass filter (12 dB per octave, 1 MHz corner frequency) and sampled by a digital oscilloscope. **d**, RTS observed when the dot gates are sufficiently energized that the QD tunnelling rate Γ lies within our 1-MHz bandwidth.